An Acad Bras Cienc (2023) 95(3): e20211594 DOI 10.1590/0001-3765202320211594
Anais da Academia Brasileira de Ciências | *Annals of the Brazilian Academy of Sciences*
Printed ISSN 0001-3765 I Online ISSN 1678-2690
www.scielo.br/aabc | www.fb.com/aabcjournal

ECOSYSTEMS

Effects of atmospheric low-level jets on the mixing process of a large tropical reservoir

ANDRÉ L. REIS, FELIPE S. PACHECO, FELIPE M. PIMENTA, ROBSON B. PASSOS, GILBERTO FISCH, JOSÉ C. MENDONÇA & ARCILAN T. ASSIREU

Abstract: Changes in the physical and biogeochemical properties of water columns are frequently associated with cold fronts and mesoscale convective systems due to increased cloud cover. The effects of low-level jet (LLJ) events on thermal stratification and water quality, however, remain undescribed, particularly for tropical reservoirs. Here, water temperature time series are combined with meteorological data, LIDAR observations, ERA5 reanalysis data, and hydrodynamical modeling to investigate the impact of an event of LLJ over the Furnas hydropower reservoir in Brazil. The LLJ event was characterized by dry, intense, and persistent winds (~10 m s-1) blowing for more than 12 hours over the main fetch of the reservoir. In the downwind side of the lake, the surface mixed layer depth increased by 50% during the LLJ event. The changes to the water column were produced by a combination of wind-induced upwelling, shear-driven mixing, and nocturnal convective overturning, different from the heat balance expected during passing cold fronts and mesoscale convective systems. The results suggest that both momentum and heat fluxes during LLJ events need to be accounted for in lake modelings to reproduce the vertical mixing process.

Key words: thermal stratification, hydrological and environmental modeling, heat fluxes, wind stress.

INTRODUCTION

Generally, wind speed increases with height above the surface. However, in some situations, the wind profile differs substantially from "standard" conditions. This is the case for low-level jet (LLJ) events, where wind speeds reach maximums not far from 200-500 m above the ground (Kalverla et al. 2019). The dynamics of LLJs are related to different atmospheric conditions, e.g., severe rainfall events (Zhao 2012, Zhong et al. 1996), air pollution (Hu et al. 2013, Mao & Talbot 2004), wind energy (Kuik et al. 2016, Porté-Agel et al. 2020), aviation safety (Fabbian et al. 2007), and low-visibility events produced by fog and air pollution (Ju et al. 2020). LLJs have been frequently observed in many continents including South America (Barros & Doyle 2018, Marengo et al. 2004, Salio et al. 2007) North America (Holt 1996, Wainwright et al. 2016, Walters et al. 2008), Europe (Baas et al. 2009, Kalverla et al. 2019), Africa (Fiedler et al. 2013, Todd et al. 2008), and Asia (Du & Chen 2019, Miao et al. 2018, Wei et al. 2013). Despite the abundant literature on the matter, investigations into the impacts of LLJs on vertical mixing processes for continental aquatic systems have not been conducted.

Vertical mixing plays an important role in the vertical structure of lakes and reservoirs,

directly influencing biophysical and chemical processes, and consequently the water quality characteristics of these reservoirs (MacIntyre et al. 2002, Reynolds 1992, Spigel & Imberger 1987). The surface mixed layer (SML) is the fraction of the water column directly impacted by surface-atmosphere interactions, and therefore sensitive to momentum and buoyancy flux (Imberger 1985). SML variability, typically modulated by diurnal to seasonal surface energy fluxes, can be suddenly disrupted by less predictable severe atmospheric processes (Tsai et al. 2008). For example, MacIntyre et al. (2002), when studying an African tropical reservoir, showed that SML deepening was enhanced due to radiative heat losses during the night and that steeper variations occurred after severe storms. By integrating observations and numerical model outputs, Kimura et al. (2012) developed a nowcasting system to understand the spatial distributions and temporal variations in the dynamics of a subtropical lake occasionally influenced by severe rainstorms. Kimura et al. (2014) determined which meteorological and environmental factors (e.g., wind, heat and freshwater inflow) controlled typhoon-induced mixing during this season. Liu et al. (2020), used high-frequency water temperature profiles at three stations in a large subtropical deep reservoir to report on the effects of rainfall on thermal stratification. They demonstrated that moderate to heavy rainfall events can reduce the thermal stability of a water column, deepening the mixed layer depth. In Brazil, Assireu et al. (2011b), studied the effect of heavy rains on the hydrographic basin for peak inflows and showed that it is an important mechanism driving thermocline displacement. Several studies have demonstrated the relationship between changes of physical and biogeochemical properties of water columns and cold fronts (CF) (Alcântara et al. 2010, Araújo et al. 2017, Curtarelli et al. 2014b, Tundisi et al. 2004). For example, Curtarelli et al. (2014b), evaluated the impacts of summertime mesoscale convective systems (MCS) on the surface mixing layer dynamics of a Brazilian Amazon hydroelectric reservoir and concluded that this process is one of the main atmospheric phenomena driving the mixing process in the Amazonian reservoir. The LLJ-induced mixing in a large Brazilian tropical hydroelectric reservoir will be evaluated, for the first time, in this article.

In this study, the effects of LLJ events on the heat balance and water thermal structure of a tropical hydropower reservoir were analyzed using *in situ* data and a three-dimensional lake model. Additionally, the possible implication for water quality was discussed. This study hypothesizes that the LLJ event induced strong turbulence on water, weakened the vertical temperature water stratification and triggered enhanced mixing along the water column which may have led to critical changes in water quality. Analysis of the LLJ effects on thermal structure and water quality of large reservoirs may contribute to the better management of tropical reservoirs by enhancing wild fisheries and aquaculture performance, promoting safe tourism and supporting decision-makers to detect the best areas for water abstraction for irrigation and human consumption.

MATERIALS AND METHODS

Description of the study site

The Furnas Reservoir is a large and deep rift valley hydroelectric reservoir in Southeast Brazil (maximum and mean depth of 90 m and 16 m, respectively, Figure 1). This is a warm monomictic water body (e.g., thermally stratified throughout much of the year experiencing, climatologically, only one overturn period per year). Furnas is located 768 m above mean sea level (maximum

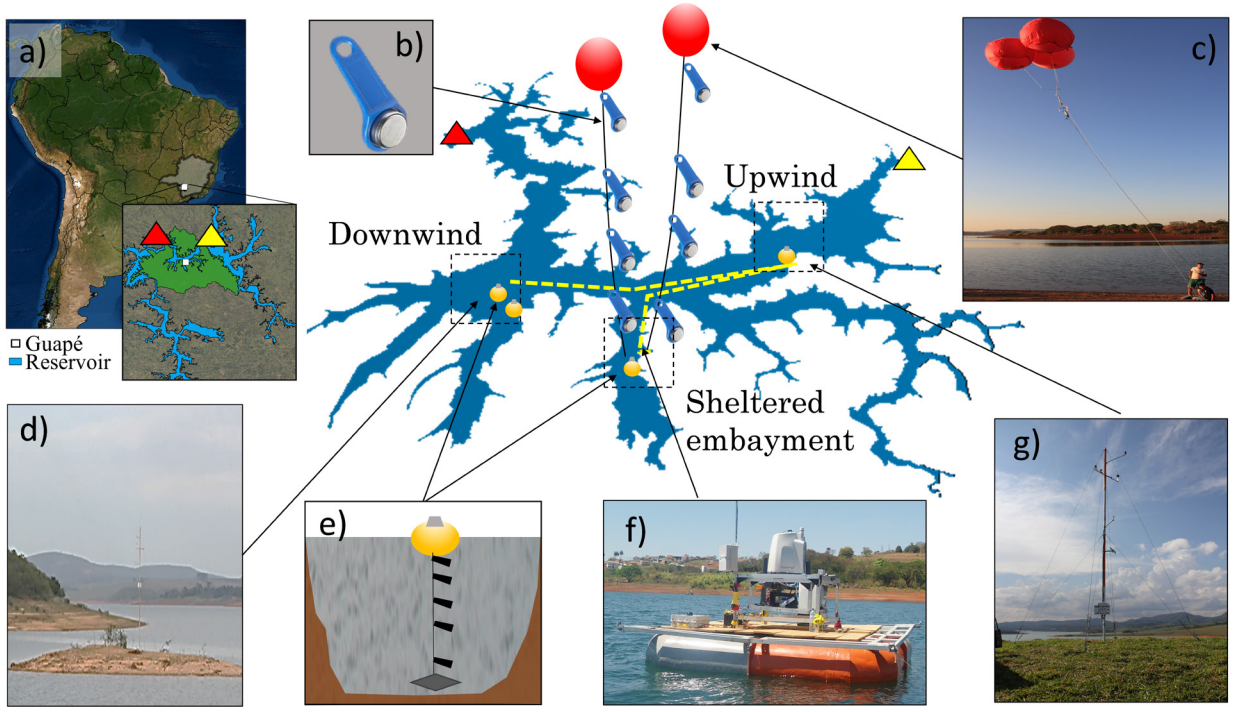

Figure 1. a) Location of the study region: the inlet (yellow triangle) and outlet (red triangle) are shown in the central panel; b) air temperature sensors fixed along a cable attached to a balloon. (c) balloons positioned on the sheltered embayment site; d) tower located on the downwind side; e) thermistor chain installed at the upwind, downwind and sheltered embayment sites; f) Lidar fixed on the float, (A yellow dashed line in the central panel illustrates the Lidar track). g) photo of the tower located on the upwind side of the reservoir on the top of a hill.

reservoir level). Its flooded area and storage capacity are 1440 km^2 and 22.95 billion m^3, respectively (FURNAS 2016). The reservoir sector studied here presents a 7 km wind fetch (Figure 1), and during the LLJ occurrence, the routine of the residents is changed, forcing for example, the ferryboat between the cities of Guapé and Capitólio to interrupt its service (Pellegrini et al. 2019). The reservoir is surrounded by 23 municipalities, 19 of which practice aquaculture. It also provides freshwater for human consumption, agriculture, industry and tourism.

Data collection

Meteorological data, water temperature and some limnological parameters were acquired along the portion of the Furnas Reservoir located near the cities of Guapé and Capitólio (Figure 1 - central panel) between September 19 and 23, 2016. Figure 1 shows the location of the four data sources used for hydro-meteorological data acquisition, including air temperature, humidity, air pressure, wind intensity, and vertical profile of water temperature and wind. Table I summarizes the sensors and their technical specifications. More details on data collection and design can be found in Assireu et al. (2019). For organizational purposes, three sites were defined along the reservoir sector: upwind (in the eastern portion), downwind (in the western portion) and a sheltered embayment (near the urban center of Guapé) (Figure 1). Time series on water temperature data were collected hourly by three thermistor chains (Figure 1e), installed upwind, downwind, and at the sheltered embayment location. Each thermistor chain had

Table I. Technical specifications of the sensors used in this study.

Sensor	Manufacture	Range	Accuracy	Depth/Height
Air temperature	Rotronic	-25 to 60 °C	± 0.3 °C	3 m
Water temperature	HOBO	-5 to 60 °C	± 0.15 °C	0.2 to 25 m
Wind speed	R.M. Young	0 to 100 ms^{-1}	± 0.3 ms-1	3 m
Wind direction	R.M. Young	0 to 360 °	± 3 °	3 m
Relative humidity	Rotronic	0 to 100 %	± 1.5 %	3 m
Barometric pressure	Vaisala	500 to 1100 hPa	± 0.3 hPa	3 m
LIDAR	Windcube V2/Leosphere	0-50 ms^{-1}	-	40 to 260 m

10 HOBO Onset@R U22-001-Water Temp Pro V2 probes (Bourne, Massachusetts, USA). These thermistors operate with a factory-specified accuracy of +/-0.2°C. At the up and downwind sites, thermistors were installed at 0.2, 2, 4, 6, 8, 10, 12, 14, 16 and 25 m depths. In the sheltered embayment, thermistors were installed in the same depths with one additional thermistor at 18 m. Air temperature data was sampled by compact sensors (Figure 1b) attached to a cable suspended by balloons inflated with helium gas (Figure 1c) and fixed near the sheltered embayment. At the downwind location a 12 m meteorological tower installed in a small island sampled air temperature, humidity and winds (Figure 1d). A Floating LIDAR platform was used in the Furnas hydroelectric reservoir experiment (Figure 1f), and the details of the sampling system can be found in (Nassif et al. 2020). A Zephir 300 LIDAR (Zephir 2014) was initially moored on the sheltered embayment site. After September 20 at 20:00h LT (UTC-3 h), it was towed along the reservoir to the downwind site. A yellow dashed line illustrates the Lidar track in the central panel of Figure 1. The Lidar remained there until 12:00h on the 22nd of September, returning to the sheltered embayment position at 14:00h the same day. LIDAR also has a coupled station called LIDAR station, and it measures temperature, humidity and atmospheric pressure.

A buoy-based system for environmental monitoring (SIMA - *Sistema Integrado de Monitoramento Ambiental*) collected meteorological data, including air temperature, humidity, atmospheric pressure, wind, and water temperature at 5, 12, 20 and 40 m depths (Stech et al. 2006). The observational data comprises hourly records from 2005 to 2007 and they were used to characterize the local climate. SIMA was located near the downwind site.

ERA5 reanalysis data and LLJs identification

The highest wind observations obtained by Lidar was 200 m (Zephir 2014). To overcome this height limitation, winds from the ERA5 (Hersbach et al. 2020) were analyzed. ERA5 is the latest reanalysis dataset from the European Centre for Medium-range Weather Forecasts (ECMWF). The choice of reanalysis data considered the high spatial, vertical and temporal resolution (0.3°, 137 vertical levels, 1 hour respectively). Kalverla et al. (2019), showed that ERA5 data from the North Sea domain demonstrates that the model can resolve low-level jets.

The wind data from the ERA5 reanalysis were used to extend the analyses of the wind fields up to 500 m. From these datasets, LLJs were identified by seeking local maxima in the wind profiles (Wei et al. 2013). After identifying the LLJs, the local maximum, jet strength, height,

and fall-off (nose of the jet) were analyzed. The fall-off is defined as the difference between the maximum and the subsequent (moving upwards) local minimum (Kalverla et al. 2019).

Data analyses

Changes in the thermal structure of a lake are controlled by the inflow and outflow contributions as well as the surface heat exchange and wind-induced mixing (Imberger & Hamblin 1982). Since no substantial variation in the reservoir level nor heavy rain events were observed during fieldwork, the inflow and outflow contribution can be neglected. To investigate the surface heat exchange impact on the thermal structure of the water column, the observed and predicted enthalpy was estimated following a methodology from Thiery et al. (2014). Enthalpy (H) measures the heat content of a system, and for H> 0 the system absorbs heat while for H < 0 the system releases heat. The observed enthalpy (Hobs) considers the time evolution of temperature distribution in the water column:

Table II. Measurements used to estimate surface heat fluxes from hourly averaged data.

Variable	Data
Air temperature	Tower at downwind site, tower at upwind site,
Water temperature	Thermistor chain
Wind speed	Tower at downwind site, tower at upwind site, LIDAR
Wind direction	tower at upwind site
Radiation	tower at upwind site
Atmospheric pressure	tower

$$H_{obs} = h\overline{\rho}cp\frac{\partial\overline{T}}{\partial t}$$

where h is the water column height, $\overline{\rho}$ is the average density of the water column, cp is the specific heat capacity of the water at constant pressure (4.1813 x 10^3 J kg^{-1} K^{-1}) and $\partial\overline{T}/\partial t$ is the average water column temperature change computed from the observed temperature profile time series data. The predicted enthalpy change H_{mod} is given by:

$$H_{mod} = R_{net} - \mathrm{LH} - \mathrm{SH}$$

where R_{net} is the net radiation, LH and SH are the turbulent fluxes of latent heat and sensible heat, respectively (all units in W/m²). The heat fluxes were determined using the "Lake Heat Flux Analyzer" (Woolway et al. 2015, Woolway 2015). This program is open source and provides heat fluxes on the surface: short-wave and long-wave radiation and sensible heat and latent heat fluxes. The Lake Heat Flux Analyzer requires a number of input variables, like air and water temperatures, relative humidity, wind speed, and short-wave radiation. The input data to calculate H_{mod} and H_{obs} are mean atmospheric measurements (Table II) and the water temperature at the sheltered embayment site.

Potential upwelling events during stratification are traditionally assessed by means of the Wedderburn Number (W) (Monismith 1986, Stevens & Lawrence 1997, Thompson & Imberger 1980) and it is a dimensionless number defined as:

$$W = \frac{g' h_1^2}{u_*^2 L}$$

Here, h_1 is the equilibrium depth of the surface layer (30 m) and L is the horizontal length of the lake (or lake fetch = 7 km), $g' = g\left(\rho_1 - \rho_2\right)/\rho_2$ is the reduced gravity due to the difference in mean water density of warmer surface and cooler lower layers (along the time) and u_* is

the shear wind velocity described by (Stevens & Lawrence 1997). For values of W < 1, there is a high probability that the thermocline will tilt sufficiently towards the surface on the upwind side, bringing hypolimnetic or metalimnetic water to the surface, and promoting shear-induced mixing with a consequent deepening of the mixing layer. According to (Shintani et al. 2010), the Wedderburn number provides a scale for the magnitude of thermocline tilt rather than an exact estimate of thermocline displacement.

Numerical model

Numerical simulations of the lake hydrodynamics were conducted with the Estuary and Lake Computer Model (ELCOM, Hodges et al. 2000). The ELCOM model is a three-dimensional numerical, hydrodynamic and thermodynamic model (Hodges & Dallimore 2016). The model was developed by the Center for Water Research (CWR) at the University of Western Australia (UWA). The hydrodynamic algorithms that are implemented in the ELCOM use a Euler-Lagrange approach for the advection of momentum adapted from Casulli & Cheng (1992), whereas the advection of scalars (e.g., tracers, conductivity and temperature) are based on the ULTIMATE QUICKEST method proposed by Leonard (1991). The thermodynamics model considers the penetrative (e.g., shortwave radiation) and non-penetrative components (e.g., longwave radiation, sensible and latent heat fluxes) (Hodges et al. 2000). The vertical mixing model uses the transport equations of turbulent kinetic energy (TKE) to compute the energy available from wind stirring and shear production for the mixing process (Spigel & Imberger 1987). A complete description of the equations and numerical methods used in the ELCOM was given by Hodges et al. (2000). ELCOM is a robust model and widely used in scientific literature capable of simulating several variables in aquatic environments, allowing researchers to understand physical processes that occur simultaneously on the surface, in the water column and in the sediments.

The simulation period was from 18 to 24 September 2016. The time step used for the calculations was 60 seconds, which was defined according to the bathymetric grid resolution and the Courant-Friedrichs-Lewy (CFL) condition (Gratziou et al. 2016). The results were programmed to be saved every 20 steps of time. The simulation domain was the stretch of the Furnas reservoir close to the municipality of Guapé given the availability of data (Figure 1). Bathymetry data were acquired from a previous study carried out in the Guapé region (Costa 2016) and re-sampled at a resolution of 100 meters using the ARCGIS 10.4 software program. The vertical resolution for all simulations was 1 meter, totaling 61 vertical layers. The water albedo was set to 0.03 (Slater 1980), and the bottom drag coefficient was set to 0.001 (Wüest & Lorke 2003). The attenuation coefficient for Photosynthetic Active Radiation (PAR) was set to 0.6 m^{-1} based on *Secchi* disc measurements. Based on a previous study conducted in another tropical reservoir (Pacheco et al. 2011), a value of 5.25 m^2 s^{-1} was chosen for the horizontal diffusivity of temperature and for the horizontal momentum.

Due to the presence of persistent unstable atmospheric conditions over tropical reservoirs (Assireu et al. 2011a, Verburg & Antenucci 2010), an atmospheric stability sub-model was activated during the simulation. This procedure was adequate because the meteorological sensors were placed within the atmospheric boundary layer (ABL) over the surface of the lake and the data were collected at sub-daily intervals (Imberger & Patterson 1989). In this manner, at each model time step, the heat and momentum transfer coefficients were adjusted

based on the atmospheric stability of the ABL. It was evaluated through the stability parameter, which was derived from the Monin-Obukhov length scale. ELCOM uses similarity functions presented by Imberger & Patterson (1989) in both stable (negative value stability parameter) and unstable conditions (positive values). The Coriolis sub-model was also activated during the simulation and the Coriolis force was then considered in the Navier-Stokes equation. This force causes the deflection of moving objects (in this case, the water currents) when they are viewed in a rotating reference frame.

Hydrodynamic simulations of the Furnas Reservoir were conducted under realistic forcing conditions (e.g., inflow, outflow, atmospheric temperature and radiation budget). Two sets of boundary cells were defined to force the inflow and outflow (Figure 1). The meteorological driving forces over the free surface of the reservoir were considered to be uniform. The model was forced using hourly averaged meteorological data (Table I) and data registered in the Weather Underground database for the 18th and 19th of September, prior to the start of data collection. The Weather Underground station data (IMINASGE82 coordinates: -21.440S -46.056O), came from the banks of the reservoir in the municipality of Alfenas-MG, which were used to compose the inputs of the model in the period prior to the 19th. The station has the seal of quality for the platform that disseminates the data. The daily inflow and outflow were provided by the National Water and Basic Sanitation Agency (ANA - http://sar.ana.gov.br).

To verify the results, a statistical analysis was applied comparing the simulated water temperature observed at the upwind, downwind and sheltered embayment sites. The Bias, Mean Square Error (MSE), the Root Mean Square Error (RMSE), the correlation index and the Nash - Sutcliffe coefficient (Nash & Sutcliffe 1970) were calculated (Table III). For the analysis of the statistics, two layers were considered (surface and deep layer), separated by a height referring to the temperature of 23.5 °C.

Table III. Statistics used. In the equations *o* represents an observed variable, *s* is a simulated variable, *n* is the number of times, and *i* is the time index.

Statistic	Equation
Bias	$\text{Bias} = \frac{1}{n}\sum_{i=1}^{n}(s_i - o_i)$
Root Mean Square Error (RMSE)	$\text{RMSE} = \sqrt{\frac{1}{n}\sum_{n=1}^{i}(s_i - o_i)^2}$
Mean Square Error (MSE)	$\text{MSE} = \frac{1}{n}\sum_{i=1}^{n}(s_i - o_i)^2$
Pearson Correlation Coefficient (r)	$r = \frac{\sum_{n=1}^{i}(s_i - \bar{o})(o - \bar{o})}{\sqrt{\sum_{n=1}^{i}(s_i - \bar{s})^2}\cdot\sqrt{\sum_{n=1}^{i}(o - \bar{o})^2}}$
Nash-Sutcliffe coefficient (E_{NS})	$E_{NS} = 1 - \frac{\sum_{i=1}^{n}(o_i - s_i)^2}{\sum_{i=}^{n}(o_i - \bar{o})^2}$

RESULTS

Characterization of local climate from *in situ* data

The precipitation data show a strong seasonal pattern defining a rainy season with precipitation above 150 mm per month from November up to March (Figure 2a). The dry season (rainfall less than 30 mm/month) is very well defined from June to August. The average wind speed ranged from 2.8 m s^{-1} to 3.0 m s^{-1} in the dry season (May to September), but decreased to 2.4 m.s^{-1} at the end of the rainy season (January to February, Figure 2a).

The monthly average air temperature in the rainy season ranges from 23°C to 25°C and decreases to 20.0°C in June-July (Figure

2b). The reduced daily (Figure 3a) and annual (Figure 3b) difference between near-surface and air temperature affects the dynamics of tropical lakes and regional climate and was previously observed in the Elqui Valley reservoir for an arid region of Chile (Bischoff-Gauß et al. 2006), for the African Great Lakes (Thiery et al. 2014), and for the Sobradinho and Furnas reservoirs located in Northeastern and mid-western Brazil, respectively (Ekhtiari et al. 2017, Gonçalves et al. 2020). The relative humidity (RH) has a seasonal pattern related to the air temperature and rainfall, but with a small shift in the minimum RH value (55 %) towards August and September (Figure 2b). Moreover, during the rainy season, the humidity can reach up to 80 % (Figure 2b). Usually, water surface temperatures (Tw) are higher than air temperatures (Ta) (Figure 3a and 3b), which tends to produce an unstable atmospheric boundary layer (ABL), as anticipated by Garratt (1994). The ABL over the Furnas reservoir remains unstable (Tw > Ta) about 5/6 of the time on an hourly scale (Figure 3a). This behavior is similar to those observed in other tropical Brazilian reservoirs (Gonçalves et al. 2020, Curtarelli et al. 2014a), and tropical lakes and reservoirs worldwide (MacIntyre et al. 2002, Verburg et al. 2011). Unstable ABL conditions were prevalent throughout most of the year, but for August and September, we observed a tendency towards neutral conditions on a monthly scale (Figure 3b).

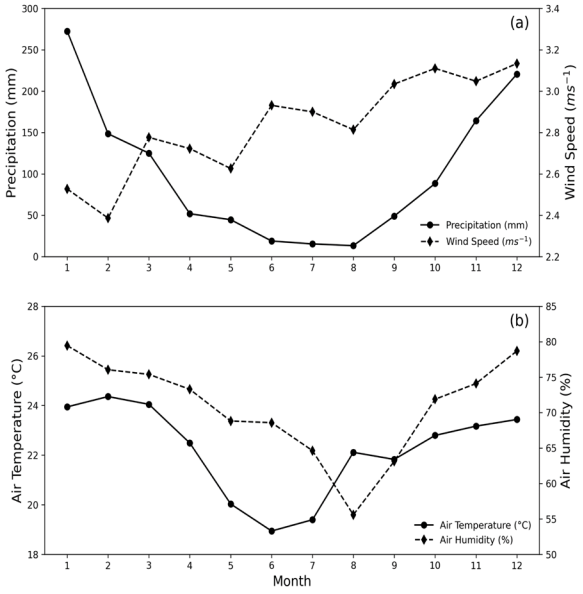

Figure 2. Climate seasonal patterns observed at the Furnas reservoir over the period of 2006-2007: monthly mean for (a) precipitation (mm month^{-1}), wind speed (m s^{-1}), (b) air temperature (°C), and humidity (%).

Environmental conditions before and during the LLJ event

At the beginning of the field experiment (before the LLJ event), winds were blowing from the southwest-southeast with moderate strength (Figure 4a). After September 21st at 21:00h LT wind strengthened reaching speeds between 8 and 11 m s^{-1} for nearly 12 hours. Winds also changed direction abruptly, blowing with a strong eastern wind maintaining this direction. After Sept 22nd at 09:00h LT, winds resumed speeds less than 5 m s^{-1} with no defined direction. Figure 4b further presents the wind speed measured by the LIDAR for all the monitored heights. Colors represent the wind speeds. Blue indicates wind speeds below 2 m s^{-1}, and red indicates wind speeds above 10 m s^{-1}. Therefore, strong (weak) wind shear can be identified by different (similar) colors and heights. The increase in the mean vertical turbulent kinetic energy (TKE) during this event (Figure 4b), is related to increased wind shear and turbulence associated with the LLJ (Kalverla et al. 2017). At the same time, a strong LLJ over the Furnas reservoir research site was shown by the ERA-5 data, with wind speeds exceeding 15 m s^{-1} at 500 m AGL (Figure 4c). This is clearly the case for LLJ, where wind speeds reached a maximum level not far (e.g. roughly less than 500 m) from the surface (Kalverla et al. 2019).

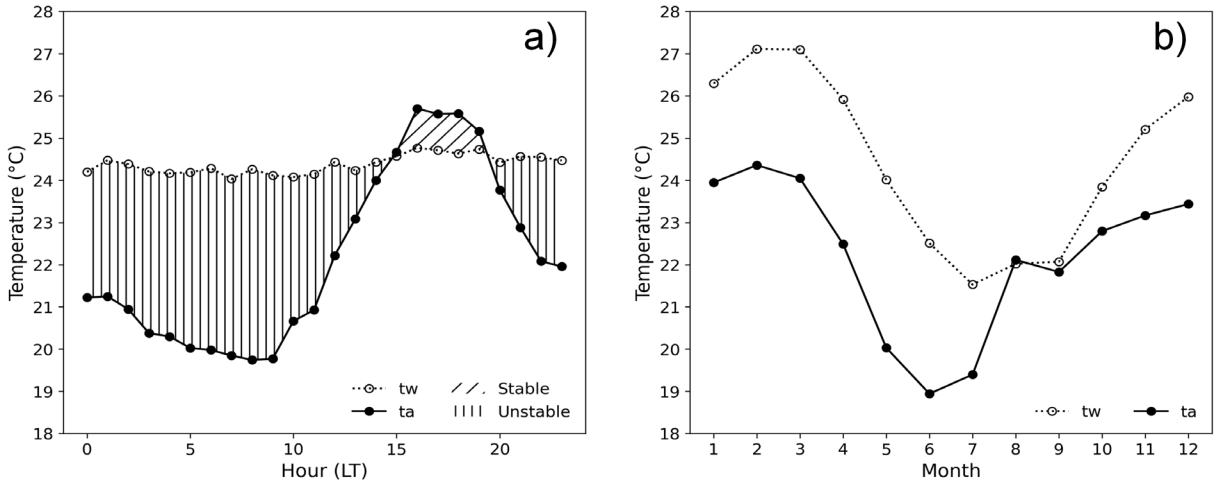

Figure 3. (a) Diurnal and (b) monthly cycle for air temperature (Ta) and water surface temperature (Tw) at the Furnas reservoir.

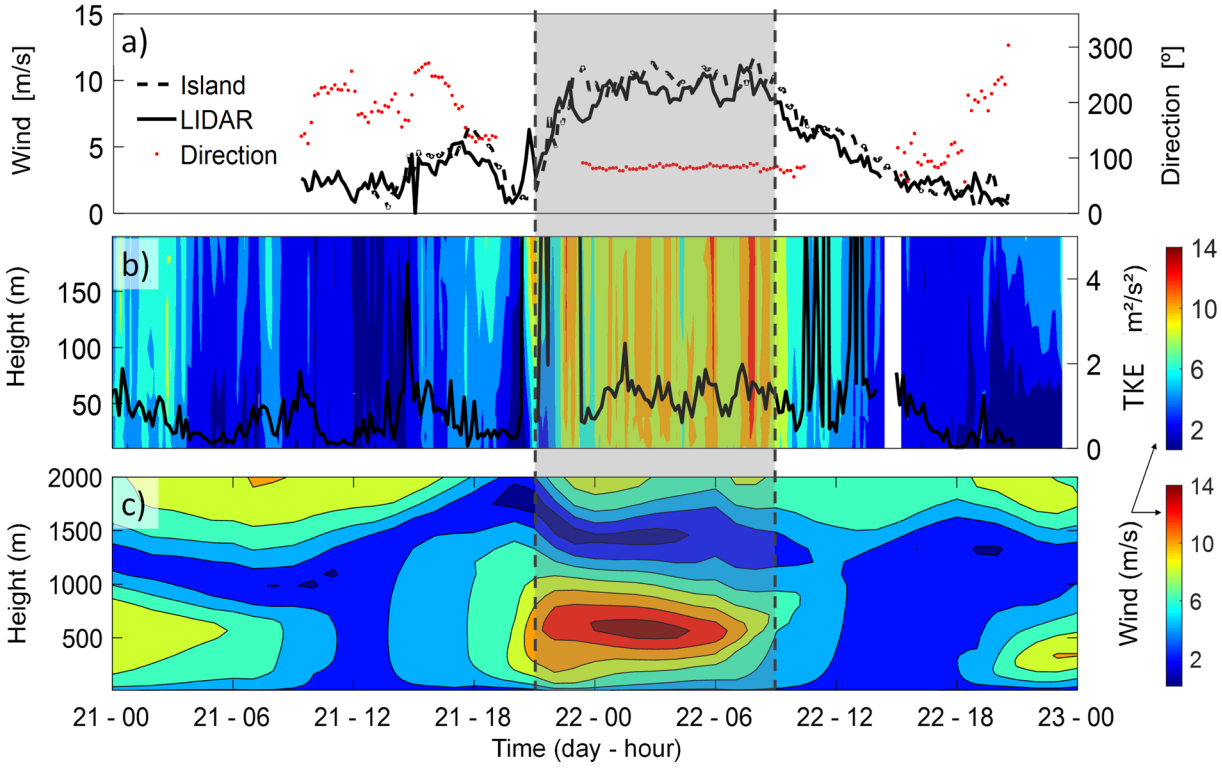

Figure 4. Meteorological conditions before and during the reported LLJ event. (a) LIDAR and anemometer wind speed time-series data for 10 m collected at the island tower and at the LIDAR position (see Figure 1), and wind direction (red) at the isle tower. Profiles of wind speed and TKE over time from LIDAR (b) and from ERA-5 data (c). The color bar indicates wind speed (m s^{-1}). The LLJ event is confined in the time window between 21:00h local time (LT), Sep. 21st and 09:00h LT, Sep. 22nd, which is marked by the dashed lines.

The relationship of this LLJ event to the atmospheric conditions was investigated by examining synoptic weather charts, prepared by the Center for Weather Forecasting and Climate Research (CPTEC) from the Brazilian National Institute for Space Research (INPE), available at www.cptec.inpe.br. These synoptic fields indicated the growing influence of an anticyclone center, initially located along the coast of Uruguay (not shown). A post-frontal high-pressure system moved northward along the southern coast of Brazil on September 21st, the measurements recorded the corresponding changes in meteorological variables. There was an increase in atmospheric pressure values to 931 hPa and a reduction of air temperatures to 13 °C, while air temperatures were around 30 °C and atmospheric pressure was around 926 hPa (Figure 5) before the LLJ. During the LLJ event, RH reached values lower than 40%.

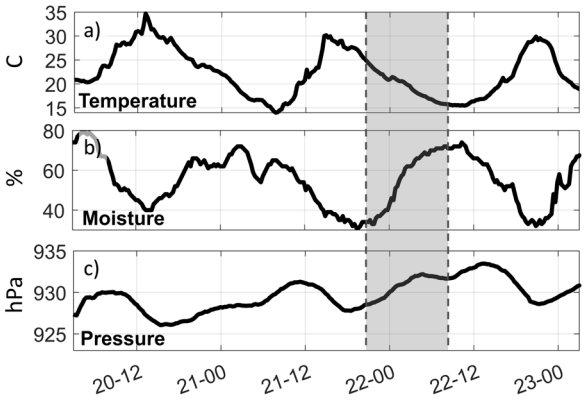

Figure 5. Hourly average temporal variations of air temperature (a), Relative humidity (b), and (c) air pressure from September 20th to September 24th.

Lake and orography effect and LLJ

Among the worldwide more documented nocturnal low-level jets (NLLJ), the South American low-level jet (SALLJ) is a larger scale phenomenon, situated in the 850-700 hPa layer, with the Amazon as the immediate moisture source and the eastern slope of the north-south elongated Andes acting to accentuate the nocturnal northerly flow (Vera et al. 2006). The relationship between SALLJ and rainfall has been noted, with the occurrence predominantly in the summer months, as exemplified by Salio et al. (2007) over northern Argentina. Articles with a substantial review on the SALLJ include Garreaud & Muñoz (2005), Marengo et al. (2004) and recently Montini et al. (2019). In our study, however, the LLJ considered is that named by Rife et al. (2010) as "weak NLLJs over the Brazilian Highlands in South American during austral winter/spring, neither of which has been previously documented". The LLJ considered here is a low-level jet which is a boundary-layer phenomenon, represented by a thin stream of fast-moving air, with maximum velocity occurring at 200-700 m above the ground. It typically develops around sunset, under clear sky conditions and strong radiative cooling, and is the result of large-scale pressure gradients, which are modified by orographic and thermal effects (Rife et al. 2010, Stensrud 1996). Although the underlying physics and synoptic processes of the formation of this event are not in the scope of this article, we will present here some evidences that the lake and its neighboring relief greatly affects this low-level jet by enhancing the along-fetch flow.

High mountains are located around the Furnas reservoir in the north and south, reaching up to 1300 m, while a relatively smoother terrain is on the east side (Figure 6a). Wind direction is affected by this orography: easterly winds blow along the lake fetch due to channeling along the lake (Figure 6b). A similar effect was observed at the Great Rift Valley in Africa, where the presence of orography greatly affects the low-level jet by enhancing the cross-equatorial flow (Chakraborty et al. 2009). Wind speed is also expected to be influenced by the intensification

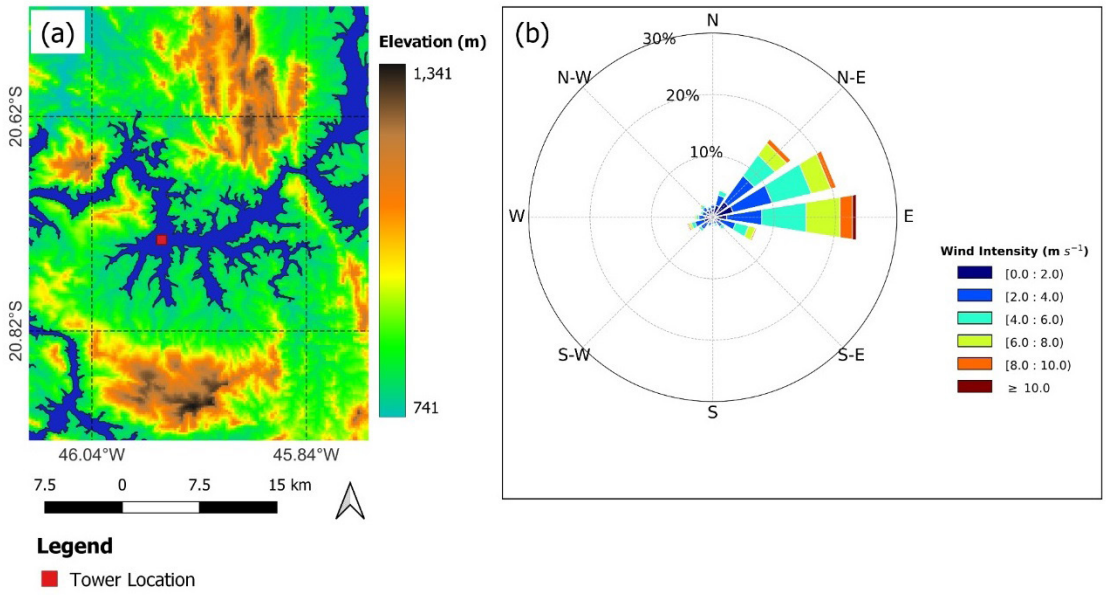

Figure 6. Surface elevation map for the study area and the locations of the upwind station (a) and the wind rose for the period studied (b).

promoted by the lake. For instance, Docquier et al. (2016) pointed out that Lake Tanganyika (East Africa) enhances wind speed by 2 m/s (~80%) as compared with the inland values. This enhanced wind speed mainly arises because of the lower roughness over lakes compared to those over lands. The authors also attribute this speed-up to the combination of wind channeling along valley mountains and wind confluence on the upwind side of the lake.

The existence of a large-scale pressure gradient, a crucial component of the boundary-layer LLJ theory, was identified both in synoptic weather charts (not shown) and ERA-5 derived fields (Figure 7a) during LLJ occurrence. Example of low-level jet profile as compared to the "standard" logarithmic wind profile where a local wind speed maxima between 500 and 700 m are identified (Figure 7b).

At Furnas reservoir, there is an interannual variability (Figure 8a) and the LLJs are more common during winter and spring than in summer (Figure 8b). The LLJ frequency of occurrence is highest between September and October and is lowest between April and May, with a maximum in October (18%) and a minimum in April (4%). The values of LLJ frequency of occurrence corresponding to each month or hour are normalized by the number of wind profiles estimated during each month or hour. An evident diurnal variation is present with LLJ frequency of occurrence increasing at night and early morning, as expected by a nocturnal-low level jet (Figure 8c).

Although the dynamical origin of nocturnal low-level jet is still under debate, some studies on the boundary layer jets in various parts of the world (e.g., Kalverla et al. 2019) shows the relation between their occurrence and atmospheric stability. However, their results based both on ERA-5 and the observations show a substantial number of jets for also unstable conditions. These authors attribute this to an artifact of the bulk Richardson number or a physical limit: "a stable atmosphere leads to a low-level jet, but the low-level jet produces wind shear, and consequently, the bulk Richardson number decreases.

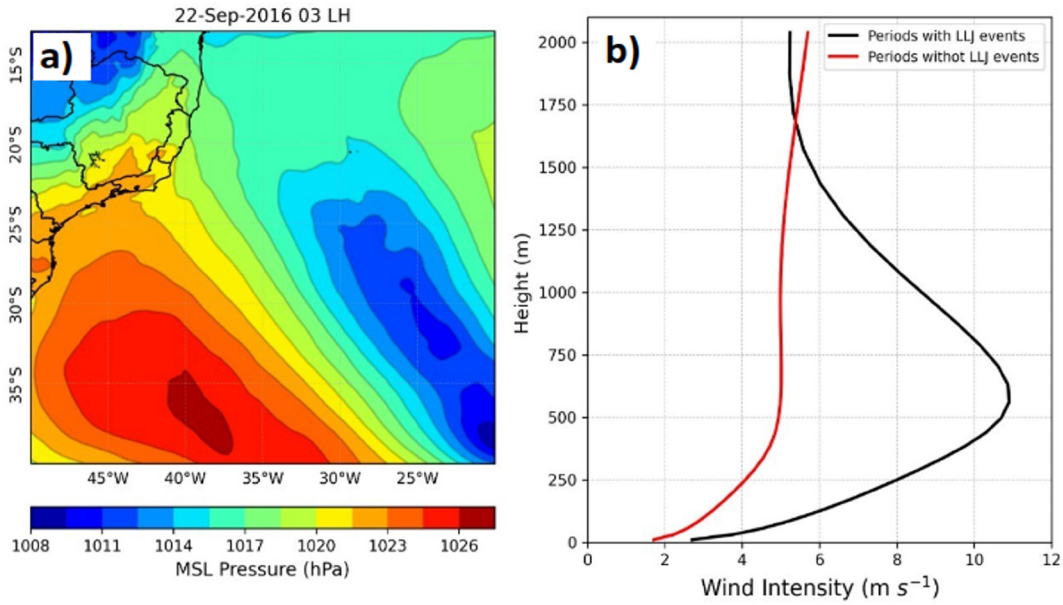

Figure 7. ERA-5 derived fields: (a) Surface pressure during the LLJ event; and (b) average vertical profiles for periods with and without LLJ event.

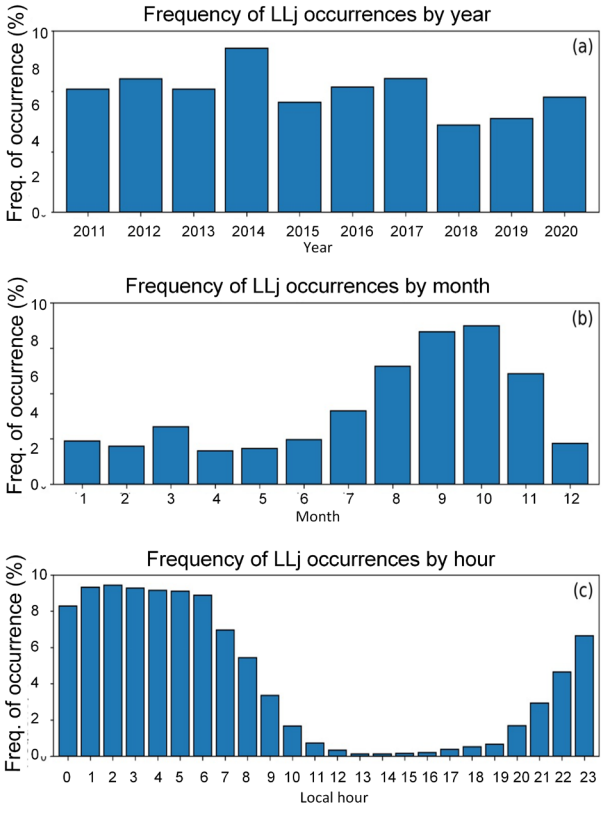

Figure 8. The long-term (a), seasonal (b) and diurnal (c) frequency of occurrence of low-level jets over ten years (2011-2020) from ERA-5 data.

Model validation

The ELCOM model performance on reservoir-atmosphere interaction at the Furnas reservoir was evaluated. The error analysis for the simulated temperature (Figure 9) showed that for the three sampled validation points (up/downwind and sheltered embayment, see Figure 1 for locations), ELCOM´s outputs tended to underestimate (bias > 0) the water temperature in the deeper layers of the water column (Figure 9a and 9c) and overestimate (bias < 0) the water temperature in the upper layers (Figure 9d and 9j). Previous studies have indicated similar behavior (Curtarelli et al. 2014a, Xu et al. 2016). For example, ELCOM applied to simulate the vertical thermal structure for a Brazilian Amazon reservoir showed a similar tendency for surface and deeper layers, as was found here (Curtarelli et al. 2014a). Xu et al. (2015), showed that the WRF-lake model generates negative biases for lake surface temperatures. They showed, for a great range of sensitivity tests, that the bias in the upper layer temperature simulations

resulted from underestimated absorption at the surface layer and the extinction of solar radiation at the lake surface. From the results at Furnas reservoir, the model gave surface layer quantities for MSE lower than 0.07 °C for the downwind and upwind points, and ranged from 0.16 °C to 0.26 °C for the sheltered embayment point. For the lower layer, the MSE values varied between 0.13 and 0.41 °C, following the same trends for the superficial layer, where the best results were observed at the main axis of the reservoir. The RMSE was lower than 0.64°C for all the validation points. The temperature measured and estimated by the model showed a correlation coefficient greater than 0.77 except for the surface layer during the LLJ event at the embayment and upwind points. The Nash-Sutcliffe efficiency index was higher than 0.7. In tropical reservoirs the vertical temperature gradients are much milder than those in temperate zones and there are temperature differences between the surface and the bottom in the order of 5°C or 6°C all year long, with a pronounced daily cycle (Missaghi et al. 2013). This difference, in the order of 5°C, coincides with what was observed at the Furnas reservoir (Figure 6). By keeping the 10% value as the tolerance error, an equivalent of ± 0.5°C was used in this study as an acceptable limit for the RMSE and MSE errors, making the error values found in this study similar to those reported in other modeling studies (Lee et al. 2013, Missaghi et al. 2013, Missaghi & Hondzo 2010, Zamani & Koch 2020). Moreover, the performance of the model during the LLJ episode maintained this acceptable limit for simulating the intense and persistent wind (Figure 9d, 9e, and 9f). This result showed that ELCOM captures instant vertical mixings observed during persistent and strong wind events, and therefore performs well when predicting the water column temperature at the Furnas reservoir.

Temporal evolution of the thermal structure

Time series data for water column temperature samples using the thermistor chains up to 25 m depth, and model results are illustrated in Figure 10. Figure 10a shows the record for the sheltered embayment station, while the upwind and downwind thermistor data are shown in Figures 10c and 10e, respectively. The analyzed period for the sheltered embayment station, started on September 20th, 2016, and ended on September 23rd, 2016, while for the upwind and downwind station, the analyzed period started on September 21st, 2016, and ended on September 22nd, 2016. Both covered the period before and during the LLJ event. The figures 10b, 10d and 10f show modeled time series of temperature for the sheltered embayment station, upwind and downwind, respectively. As anticipated in others studies (Alcântara et al. 2010, Lorenzzetti et al. 2015), Brazilian tropical reservoirs typically have heat sinks from October to February that act as heat sources from June to September, which coincides with higher wind periods in these aquatic systems (Assireu et al. 2011b). This explains the moderate stratification, near 5°C, difference between the epilimnion and hypolimnion, that coincides with the values observed at large Brazilian Amazonian reservoirs (Curtarelli et al. 2014b), tropical savanna reservoirs (Curtarelli et al. 2014a), and at the Furnas reservoir during September 2013 and 2014 (Araújo et al. 2017). Since strong wind speeds can promote vertical mixing, it was expected that the LLJ would alter the mixed characteristics. The mean diel pattern for temperatures in the upper layers (before LLJ occurrence) (Figure 10a) is strongly modulated by the surface water that is warmed by the solar radiation, showing higher values at 15:00h LT and minimum values at 06:00h LT, corresponding to the end times of net heat gains and losses, respectively. Daytime vertical temperature differences developed in

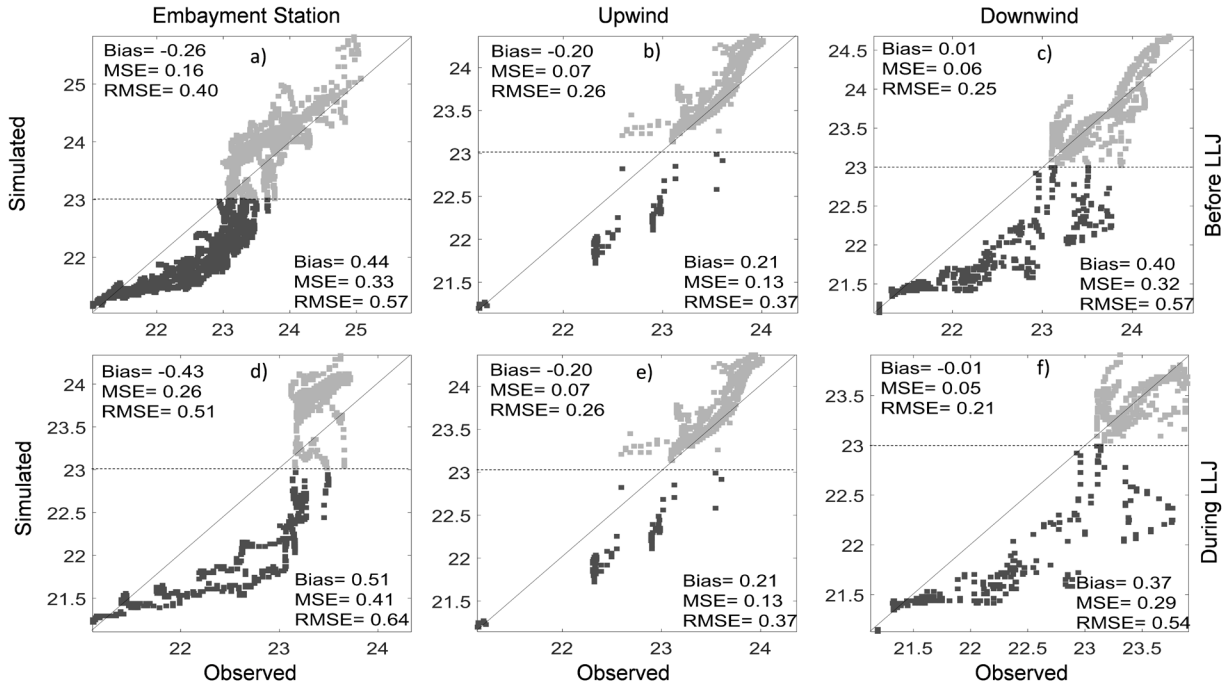

Figure 9. Three-dimensional model validation: (a) sheltered embayment station, (b) upwind station, (c) downwind station, all data collected before the LLJ, (d) sheltered embayment station, (e) upwind station, and (f) downwind station, all data during LLJ event.

the water column ranging from 3°C at 06:00 h (LT) to 4.5°C at 16:00h LT, while during and after the LLJ event this variation dropped to 1.5°C at the downwind station and 3.0°C at the upwind station. Except for the upwind side of the reservoir (Figure 10b), a pronounced tilt in the thermocline was observed (Figure 10a and 10c) in response to the action of intense and persistent winds pushing surface waters in the direction of the wind (Figure 12b).

The water column temperature time series shows variations similar to the observations. The maximums are observed around 15:00h LT and the minimums around 06:00h HL. During the LLJ, a deepening of the mixed layer was observed in the sheltered embayment and downwind station (Figure 10b and 10d), and a shallower mixed layer on the upwind side (Figure 10f). The deepening of the mixing layer observed at the downwind site (Figure 10e) was more abrupt than that modeled (Figure 10f). Accompanying the results of the observations, the temperature differences in the water column decreased after the LLJ.

It is well known that wind-induced stirring at water surfaces in aquatic systems is fetch-dependent (Sherman et al. 1978, Stone et al. 2019). To explore the mechanisms that might explain the abrupt and intense mixing between the epilimnion and metalimnion water observed here, the conditions where upwelling was likely to occur was investigated. Figure 8 shows the thermocline depth and the Wedderburn number evolution as a function of time. Using a 22.5 °C isotherm as the thermocline depth for the upwind, downwind and sheltered embayment locations, we observed that the thermocline depth changed from 8 m before the event to nearly 20 m during the LLJ event on the downwind side of the reservoir. During the LLJ event, the

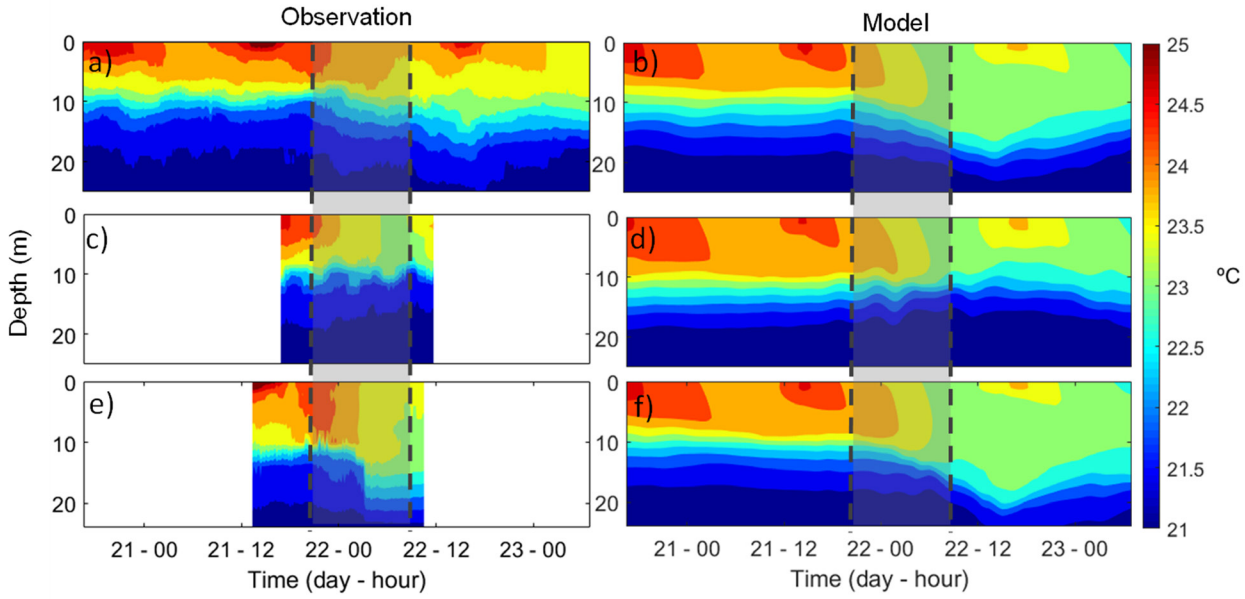

Figure 10. Time series data on water column temperatures observed and modeled at the sheltered embayment station (a - b), the upwind station (c - d), and the downwind station (e - f). The vertical dash bars indicate the LLJ event window.

Wedderburn number (W) was persistently less than one for the entire LLJ duration period (Figure 11b). As anticipated by Monismith (1986), and Imberger (1985), for values of W < 1, there is a high probability that the tilt of the thermocline is severe enough for a total upwelling on the upwind side of the reservoir and deepening of the thermocline on the downwind side (Figure 11b).

This will lead to enhanced mixing on the upwind side of the reservoir by a different mechanism than a shear-induced process. Blanton (1973), and Monismith (1986), describe this mechanism as *edge leakage*. As heavier upwelled fluid is incorporated into the near-surface (Figure 10b), it flows over lighter surface waters, leading to density inversions, thus enhancing the turbulence and mixing. W values tended to be larger before and after the LLJ event (Figure 10).

Before the LLJ, the water temperatures at the reservoir surface and at 10 m below the surface tended to be spatially heterogeneous in the afternoon period, creating a weak horizontal temperature gradient between the littoral and pelagic zones in the Furnas reservoir (Figure 12a and 12b). This scenario changed due to the LLJ event (Figure 12c and 12d). This spatial heterogeneity, particularly at the surface layer (Figure 12c), decreased during the LLJ event when the water was cooler than before. The difference between the water temperature before and during the LLJ event reached 1.5°C (Figure 12c and 12f). This decreased horizontal temperature gradient observed during the LLJ event can be explained by the higher horizontal currents induced by the winds on the reservoir surface.

The time evolution in the water shear velocity, U*, associated with the generation of TKE before and during the LLJ event (Figure 13a), showed that U* ranged from 0 to 1.5 cm/s, with a mean value of 0.7 cm/s. The diel behavior showed higher values occurring during the nighttime and early morning and lower values occurring during the afternoon. An abrupt and intense increase in U* values was observed during the

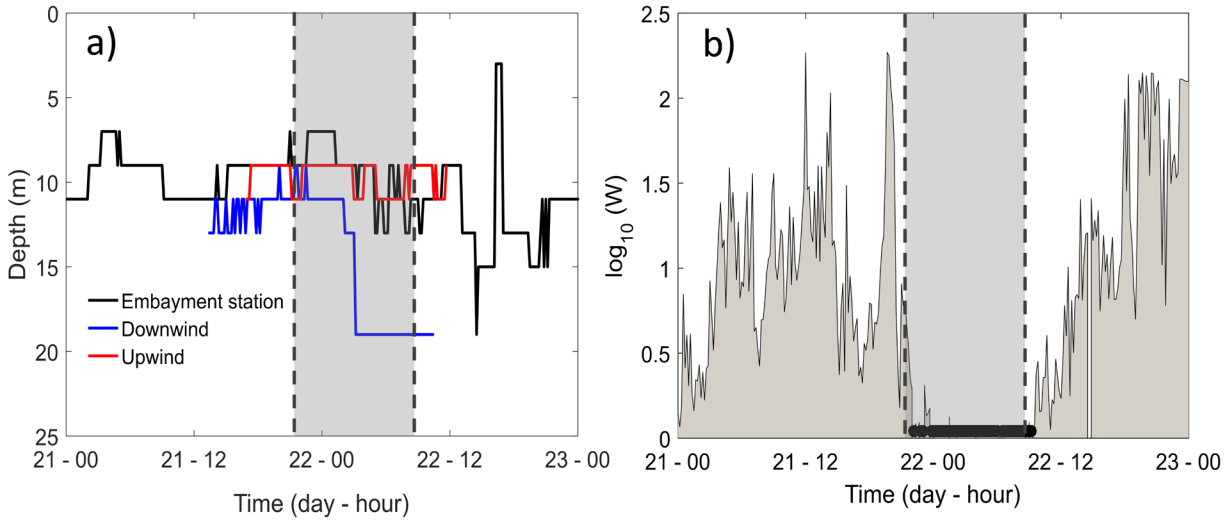

Figure 11. Time evolution of (a) thermocline depth, and (b) Wedderburn number (W). Full upwelling expected during wind events where W<1, as indicated by the black dotted lines.

LLJ event, indicating that most TKE available for mixing the water column was generated by wind shear. As anticipated in Section Data analyses we used the enthalpy change (Thiery et al. 2014), to investigate the main source of the TKE (e.g., wind stirring or surface cooling), controlling the deepening of the thermocline during the LLJ event. Time variations in the water column stratification can be attributed to meteorological variability and associated changes in the reservoir energy budget. Comparisons of hourly averages showed enthalpy changes (H_{obs}), and predicted enthalpy changes (H_{mod}) (Figure 13b) shows that the observations (H_{obs}) were captured well using the model outputs (H_{mod}) during the day. During the period of observation, enhanced solar radiation reaches the reservoir surface, increasing the amount of energy available to stratify the near-surface layer during the late morning and early afternoon. For this period of the day both H_{obs} and H_{mod} show similar variability, and therefore reproduce enhanced stratification. However, H_{obs} was not reproduced by H_{mod} during the night, when the winds are more intense. Particularly during the LLJ event, H_{mod} failed to reproduce the column-integrated water temperature as shown in Figure 13b. This showed that other mechanisms different from those that are related to surface energy balance dominated the time evolution of the thermal vertical structure during the LLJ event. Previous studies have stated that no models include mechanisms to account for diffusivity generated by upwards motion of the whole water column (Schmid et al. 2005, 2010).

DISCUSSION

Previous studies have pointed out that the mixed layer deepens during mesoscale convective system (MCS) and cold fronts (CF), and is primarily driven by subtle changes in cloud cover and incident short wave radiation (Alcântara et al. 2010, Araújo et al. 2017, Curtarelli et al. 2014a, b, MacIntyre et al. 2002). The hourly mean heat fluxes for the day before and during LLJ activity over the Furnas reservoir (Figure 14d) show that impacts of the LLJ on heat fluxes

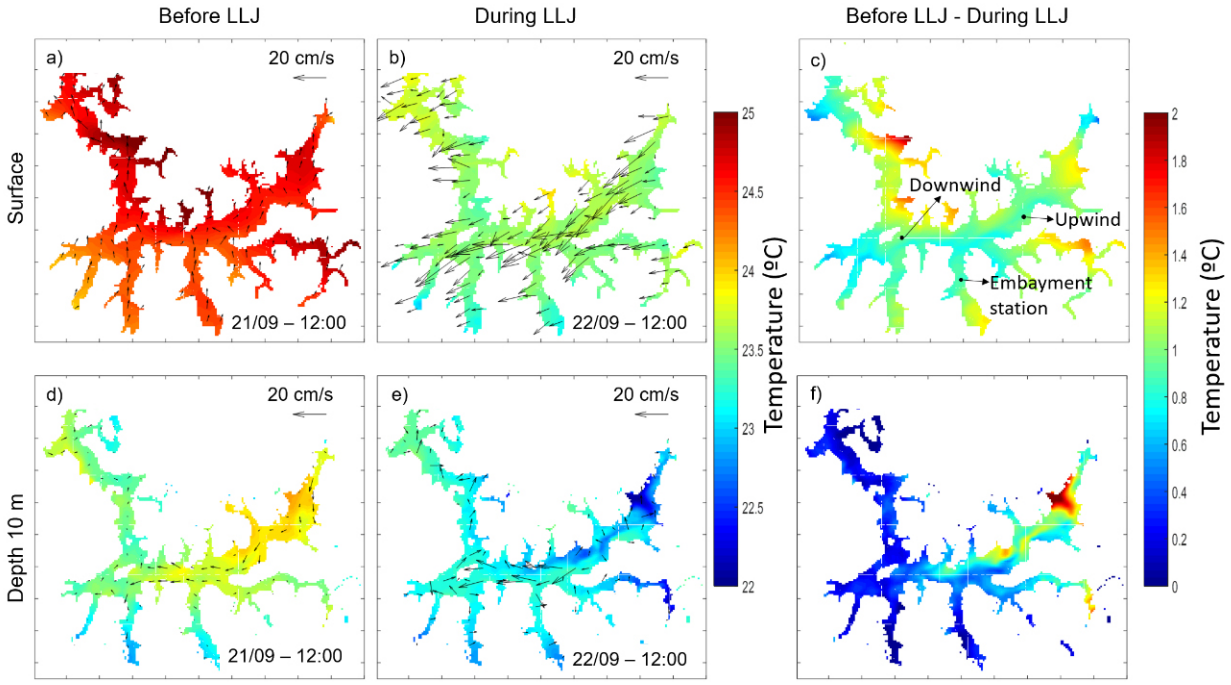

Figure 12. Spatiotemporal water temperature and speed simulated at the surface for one day before the LLJ event (September 21st 2016) (a), during the LLJ event (b), the differences (c), the same for 10-m depth before the LLJ event (d), during the LLJ event (e), and the differences (f). The locations of thermistor chains are shown in the c panel.

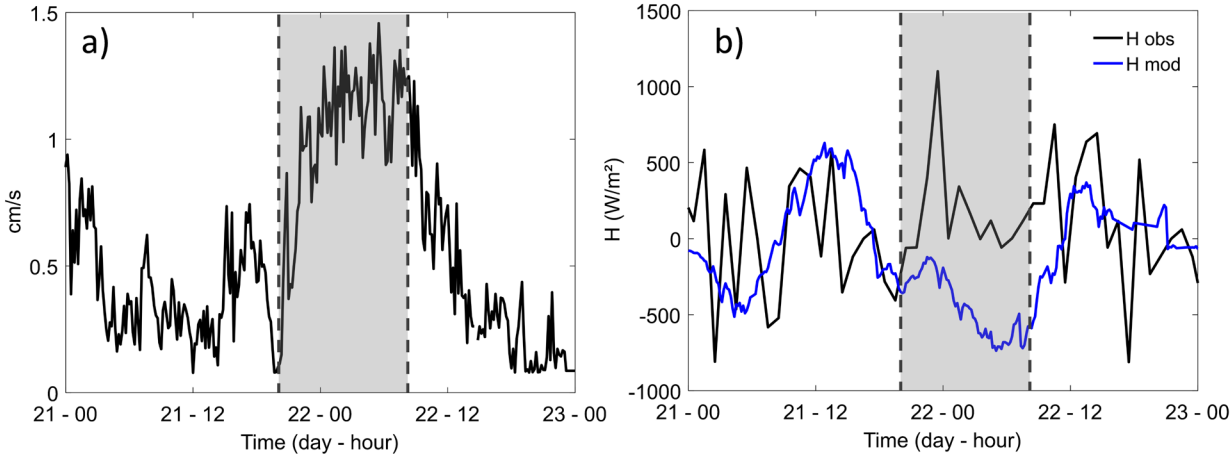

Figure 13. Time series of (a) wind shear velocity, and (b) lake enthalpy change.

are significantly different for cold fronts and mesoscale convective systems. Similar to the results presented by these previous studies, some remarkable differences from surface energy balance during the LLJ event were noticed:

1) No variation for the shortwave radiation between days with or without LLJ events, while an abrupt decrease in this parameter was observed for both CF and MCS action;
2) sensible heat flux during the LLJ event was nearly 5 times greater than that observed during MCS and CF activity;
3) the latent heat flux during the LLJ event was nearly four times greater than that observed during CF and more than five times that of MCS.

This enhanced increase in the latent heat flux is driven by the joint action of the significantly reduced relative humidity (RH) typical for dry season (Fig. 2 and 5) and the persistent and intense winds typical during the LLJ event, which draws attention to the enhanced-evaporative process during the LLJ event. Thus, different from the results of the previously cited studies, the changes observed in the heat balance components during LLJ activity were mainly driven by the combined effect between high and persistent winds and reduced values of RH, instead of the increase in the cloud cover with the consequent reduction of incident shortwave radiation over the water.

In response to the persistence and intense wind and abrupt decrease in the air temperature engendered by the LLJ event, the net reservoir heat balance becomes strongly negative (reservoir heat radiative loss) compared with the previous day without LLJ. During this event, the mixing layer exhibited a distinct behavior before and during the LLJ (Figure 14a, 14b, and 14c). The LLJ event produced surface water temperatures < 23°C at the main body of the reservoir, where this isotherm is typically between 10 m and 15 m deep. A rapid change in the water temperature over the 10 m depth was observed in the main body of the reservoir (Figure 14a, and 1b), while for the sheltered station (Figure 14) this variation was less pronounced. However, a sensitive thermocline tilt can be observed in this embayment. This result points out that the response of the water to the LLJ action is fetch dependent. As indicated in the results, the combined effect of the upwelling and the sudden increase in the reservoir heat radiative loss, mainly in the form of latent heat, engendered this dynamic observed in the water column.

Impacts for aquatic ecology

Sudden changes in the water temperature may have important ecological consequences for pelagic communities (Lisi & Schindler 2015). The Furnas reservoir is widely used for sport fishing and intensive fish farming. Although the thermal fluctuation effect on fish growth is not well understood (Azaza et al. 2010), increasing evidence suggests that the temporal variability, besides the lethal limits to specific organisms, is equally important to the health of aquatic ectothermic species (Olden & Naiman 2010, Steel et al. 2012, Vasseur et al. 2014). The municipalities surrounding lake Furnas receive thousands of tourists per year translating to significant gains for the local economy. Local sportfishing guides acknowledge that large wind storms create unfavorable fishing conditions for 1-3 days following an intense and persistent wind. We suggest that these poor fishing conditions may be related to stressful conditions induced by the sudden fluctuation in reservoir temperatures, as indicated in our results. Araújo et al. 2017, evaluated the implications of atmospheric cold fronts on the aquaculture of Nile tilapia *Oreochromis niloticus* (L.) in net fish farming regions in the Furnas reservoir. In their

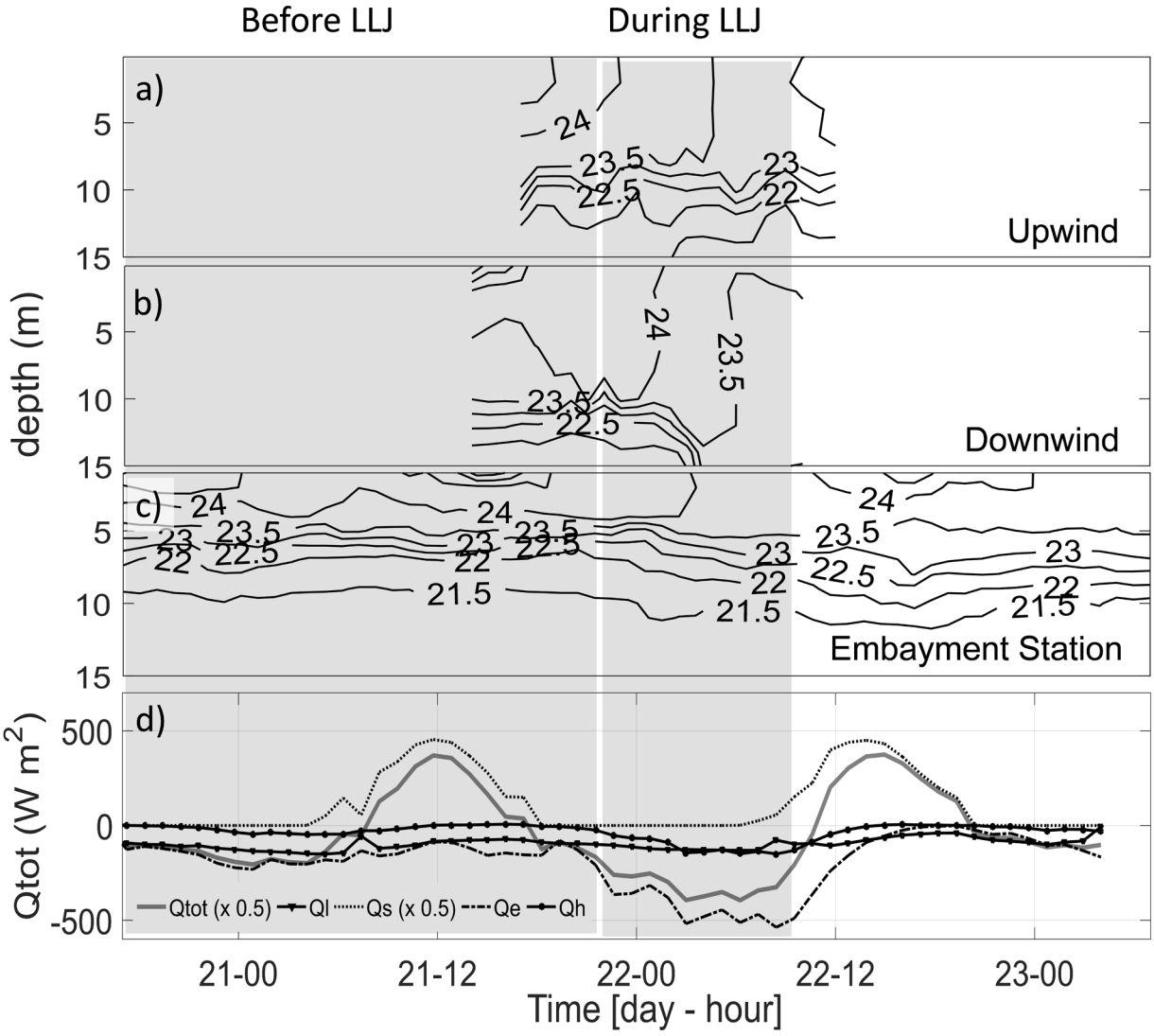

Figure 14. **Mixing layer dynamics at the main body of the reservoir (up and downwind station) (a, b) and embayment station (c). Time series data on surface heat flux components: latent heat flux (Qe), longwave net radiation (Ql), sensible heat flux (Qh), total heat balance (Qtot), and shortwave radiation (Qs) (d) for days before and during LLJ activity.**

study, the authors did not observe any critical changes in water quality parameters, interesting to aquaculture fields, that would adversely affect Nile tilapia cultivation. They argue that the absence of a well-developed hypolimnion and not completely eroded stratification could be the explanation. Our results partially corroborate their results, since they show that, for the sheltered station, the mixing process was rather modest, when compared to what has been measured along the main body of the reservoir. Thus, these results indicate that intensive cultivation of Nile tilapia should be positioned on the embayment and never in the main body of the reservoir. The embayment site is surrounded by complex terrain associated

with a decrease in local surface wind that leads to weaker mechanical turbulence, resulting in less latent heat exchange. In addition, the embayment is less subject to vertical water movement, since upwelling is a fetch-dependent process.

Stratified reservoirs often have large differences in nutrients and dissolved oxygen above and below the thermocline (MacIntyre et al. 1999). Mixing chemically different layers may occur as a response to atmospheric forcing (Hingsamer et al. 2014). Tundisi et al. (2010), indicate that, for tropical lakes and reservoirs, increases in nutrients related to the intense vertical mixing during meteorological disturbances creates a pre algae bloom condition in the upper part of the water column. Thus, the reservoir response to LLJ action can play a key role in driving the water quality and Green House Gas (GHG) emissions of large reservoirs, since they promote partial or entire mixing of the water column.

Recent studies have shown that there are significant differences in GHG gas emissions during water mixing processes (Bastien 2011, Beaulieu et al. 2014, Demarty & Bastien 2011). The carbon dioxide (CO2) fluxes estimated by the ELCOM model (not shown), indicate that fluxes can be approximately 3 times higher during LLJ events when compared with a stably stratified period. The results of this study indicate that LLJ has the potential to promote the upwelling of deep waters, which can result in pulse emissions where gases that have accumulated under the thermocline are suddenly mixed upward and vented into the atmosphere.

CONCLUSION

According to the analyses of the water temperature profiles, combined with the meteorological mast, the LIDAR observations, the ERA5 reanalysis data, and the three-dimensional (3-D) water quality modeling, we evaluated a severe LLJ-induced mixing event in a large tropical reservoir. The main conclusions are as follows:

1) The analyses suggest that LLJ events cool the surface water through enhanced latent heat flux (LH) combined with shear-induced mixing and full upwelling. The *edge leakage* mechanism was presumably responsible for enhanced mixing on the upwind side. The increased LH loss is driven by an enhanced-evaporative process due to the reduced relative humidity (RH), and intense winds observed during the LLJ event.
2) Impacts of LLJ on heat fluxes is significantly different than cold fronts (CF) and mesoscale convective systems (MCS). The heat balance components during LLJ activity were mainly driven by the combined effect of high and persistent winds with reduced RH values, instead of the increase in the cloud cover with consequent reductions in shortwave radiation on the water, as was the case for CF and MCS.
3) A rapid change in the water temperature deeper than 10 m was observed in the main body of the reservoir, while for the sheltered station this variation was less pronounced. As a consequence, the embayment site is less subject to vertical water movement, since upwelling is a fetch-dependent process. These results indicate that intensive cultivation of Nile tilapia, as is practiced at this reservoir, should be positioned in the embayment and never in the main body of the reservoir. This result is very interesting, especially in light of the current conjecture, where Brazilian reservoirs are undergoing critical condition changes with respect to their water storage capacity. This scenario should force fish farmers to move

their cultivations to the main body of the reservoir. If our results are correct, this could have a very negative impact on this activity when LLJ events occur.

4) The reservoir response to LLJ events can play a key role in driving water quality and GHG emissions in large reservoirs, since the response promotes the upwelling of deep waters, which can result in pulse emissions where gases that have accumulated under the thermocline are suddenly mixed upward and vented to the atmosphere. Therefore, the LLJ events contribute to the carbon flux of reservoirs which is important and should be included in models for regional and global carbon cycling.
5) The high and persistent wind from LLJ changes the routines of residents and tourists, forcing for example, ferryboat services between Guapé and Capitólio to be interrupted. Studies on implementing a waterway in the reservoir linking Formiga and Alfenas, at a distance close to 200 km, are currently underway. Ports have also been projected along this route to assist other cities in the area.

The results presented here have the potential to contribute to the safe and efficient management of this waterway. The underlying physics and synoptic processes related to the formation of the LLJ reported here are under investigation and will be communicated later.

Acknowledgments

A.L.R would like to thank the Coordenação de Aperfeiçoamento de Pessoal de Nível Superior (CAPES) for the master's scholarship. A.T.A. would like to thank the Conselho Nacional de Desenvolvimento Científico e Tecnológico (CNPq) (431602/2018-2, 311840/2018-3) and Fundação de Amparo à Pesquisa do Estado de Minas Gerais (FAPEMIG) (APQ 1575/14, APQ-03328-17). F.M.P. and A.T.A. would like to acknowledge Project MOVLIDAR and INEOF/INCT from CNPq (406801/2013-4, 311930/2016-6 and 465672/2014-0).

REFERENCES

ALCÂNTARA EH, STECH, JL, LORENZZETTI JA, BONNET MP, CASAMITJANA X, ASSIREU AT & MORAES NOVO EML. 2010. Remote sensing of water surface temperature and heat flux over a tropical hydroelectric reservoir. Remote Sens Environ 114: 2651-2665.

ARAÚJO C, SAMPAIO F, ALCANTARA E, CURTARELLI M, OGASHAWARA I & STECH J. 2017. Effects of atmospheric cold fronts on stratification and water quality of a tropical reservoir: Implications for aquaculture. Aquacult Environ 9: 385-403.

ASSIREU A, PIMENTA F & SOUZA V. 2011a. Assessment of the wind power potential of hydroelectric reservoirs. Energy Res Dev Distrib Exploit 1: 1-28.

ASSIREU AT ALCÂNTARA E, MORAES NOVO EML, ROLAND F, PACHECO FS, STECH JL & LORENZZETTI JA. 2011b. Hydro-physical processes at the plunge point: an analysis using satellite and in situ data. Hydrol Earth Syst Sci 15: 3689-3700.

ASSIREU AT, MENDONÇA JC, FREITAS RM, REIS AL, PELLEGRINI CC & PIMENTA FM. 2019. Uso de VANT para prospecção eólica em sistemas aquáticos: Desenho amostral e avanços instrumentais. Rev Bras Meteorol 34: 237-245.

AZAZA MS, LEGENDRE M, KRAIEM MM & BARAS E. 2010. Size-dependent effects of daily thermal fluctuations on the growth and size heterogeneity of Nile tilapia Oreochromis niloticus. J Fish Biol 76: 669-683.

BAAS P, BOSVELD FC, BALTINK HK & HOLTSLAG AAM. 2009. A Climatology of Nocturnal Low-Level Jets at Cabauw. J Appl Meteorol 48: 1627-1642.

BARROS VR & DOYLE ME. 2018. Low-level circulation and precipitation simulated by CMIP5 GCMS over southeastern South America. Int J Climatol 38: 5476-5490.

BASTIEN J. 2011. CO2 and CH4 diffusive and degassing fluxes from 2003 to 2009 at Eastmain 1 reservoir, Québec, Canada. Inland Waters 1: 113-123.

BEAULIEU JJ, SMOLENSKI RL, NIETCH CT, TOWNSEND-SMALL A & ELOVITZ MS. 2014. High Methane Emissions from a Midlatitude Reservoir Draining an Agricultural Watershed. Environ Sci Technol 48: 11100-11108.

BISCHOFF-GAUSS I, KALTHOFF N & FIEBIG-WITTMAACK M. 2006. The influence of a storage lake in the Arid Elqui Valley in Chile on local climate. Theor Appl Climatol 85: 227-241.

BLANTON JO. 1973. Vertical entrainment into the epilimnia of stratified lakes. Limnol Oceanogr 18: 697-704.

CASULLI V & CHENG RT. 1992. Semi-implicit finite difference methods for three-dimensional shallow water flow. Int J Numer Methods Fluids 15: 629-648.

CHAKRABORTY A, NANJUNDIAH RS & SRINIVASAN J. 2009. Impact of African orography and the Indian summer monsoon on the low-level Somali jet. Int J Climatol 29: 983-992.

COSTA DA. 2016. Uso De Dados Termais Orbitais No Modelo ELCOM Para a Região De Guapé (MG) Do Reservatório De Furnas [Instituto Nacional de Pesquisas Espaciais]. http://urlib.net/8JMKD3MGP3W34P/3LLNF7H.

CURTARELLI MP, ALCÂNTARA EH, RENNÓ CD & STECH JL. 2014a. Physical changes within a large tropical hydroelectric reservoir induced by wintertime cold front activity. Hydrol Earth Syst Sci 18: 3079-3093.

CURTARELLI MP, OGASHAWARA I, ARAÚJO CAS, ALCÂNTARA EH, LORENZZETTI JA & STECH JL. 2014b. Influence of summertime mesoscale convective systems on the heat balance and surface mixed layer dynamics of a large Amazonian hydroelectric reservoir. J Geophys Res: Ocean 119: 8472-8494.

DEMARTY M & BASTIEN J. 2011. GHG emissions from hydroelectric reservoirs in tropical and equatorial regions: Review of 20 years of CH4 emission measurements. Energy Policy 39: 4197-4206.

DOCQUIE D, THIERY W, LHERMITTE S & VAN LIPZIG N. 2016. Multi-year wind dynamics around Lake Tanganyika. Clim Dyn 47: 3191-3202.

DU Y & CHEN G. 2019. Climatology of low-level jets and their impact on rainfall over southern China during the early-summer rainy season. J Climate 32: 8813-8833.

EKHTIARI N, GROSSMAN-CLARKE S, KOCH H, SOUZA W, DONNER RV & VOLKHOLZ J. 2017. Effects of the Lake Sobradinho Reservoir (Northeastern Brazil) on the Regional Climate. Climate 5.

FABBIAN D, DE DEAR R & LELLYETT S. 2007. Application of Artificial Neural Network Forecasts to Predict Fog at Canberra International Airport. Weather Forecast 22: 372-381.

FIEDLER S, SCHEPANSKI K, HEINOLD B, KNIPPERTZ P & TEGEN I. 2013. Climatology of nocturnal low-level jets over North Africa and implications for modeling mineral dust emission. J Geophys Res: Atmospheres 118: 6100-6121.

FURNAS. 2016. Usina de Furnas. Dados Técnicos. https://www.furnas.com.br/subsecao/120/usina-de-furnas---1216-mw?culture=pt.

GARRATT JR. 1994. The atmospheric boundary layer. Earth Sci Rev 37: 89-134.

GARREAUD R & MUÑOZ RC. 2005. The Low-Level Jet off the West Coast of Subtropical South America: Structure and Variability. Mon Weather Rev 133: 2246-2261.

GONÇALVES AR ET AL. 2020. Enhancement of Cloudless Skies Frequency over a Large Tropical Reservoir in Brazil. Remote Sens 12.

GRATZIOU M, KOPASAKIS K & CHALATSI M. 2016. Study of the hydrodynamic characteristics of a Mediterranean stabilization ponds system using a 3D hydrodynamic model. Eur Water 53: 55-70.

HERSBACH H ET AL. 2020. The ERA5 global reanalysis. Quarterly Journal of the Q J R Meteorol Soc 146: 1999-2049.

HINGSAMER P, PEETERS F & HOFMANN H. 2014. The Consequences of Internal Waves for Phytoplankton Focusing on the Distribution and Production of Planktothrix rubescens. PLoS ONE 9: 1-17.

HODGES B & DALLIMORE C. 2016. Estuary, Lake and Coastal Ocean Model User Guide. In Users Guide, p. 1-2

HODGES BR, IMBERGER J, SAGGIO A & WINTERS KB. 2000. Modeling basin-scale internal waves in a stratified lake. Limnol Oceanogr 45: 1603-1620.

HOLT T. 1996. Mesoscale forcing of a boundary layer jet along the California coast. J Geophys Res 101: 4235-4254.

HU XM, KLEIN PM, XUE M, LUNDQUIST JK, ZHANG F & QI Y. 2013. Impact of Low-Level Jets on the Nocturnal Urban Heat Island Intensity in Oklahoma City. J Appl Meteorol Climatol 52: 1779-1802.

IMBERGER J. 1985. The diurnal mixed layer1. Limnol Oceanogr 30: 737-770.

IMBERGER J & HAMBLIN PF. 1982. Dynamics of Lakes, Reservoirs, and Cooling Ponds. Annu Rev Fluid Mech 14: 153-187.

IMBERGER J & PATTERSON JC. 1989. Physical Limnology (Hutchinson JW & T.Y. B.T.-A. in. Wu AM (Eds), Elsevier 27: 303-475.

JU T, WU B, WANG Z, LIU J, CHEN D & ZHANG H. 2020. Relationships between Low-Level Jet and Low Visibility Associated with Precipitation, Air Pollution, and Fog in Tianjin. Atmosphere 11: 1-21.

KALVERLA PC, DUNCAN JR JB, STEENEVELD GJ & HOLTSLAG AAM. 2019. Low-level jets over the North Sea based on ERA5 and observations: together they do better. Wind Energy Sci 4: 193-209.

KALVERLA PC, STEENEVELD GJ, RONDA RJ & HOLTSLAG AAM. 2017. An observational climatology of anomalous wind events at offshore meteomast IJmuiden (North Sea). J Wind Eng Ind Aerodyn 165: 86-99.

KIMURA N, LIU WC, CHIU CY & KRATZ TK. 2014. Assessing the effects of severe rainstorm-induced mixing on a

subtropical, subalpine lake. Environ Monit Assess 186: 3091-3114.

KIMURA N, LIU WC, CHIU CY, KRATZ TK & CHEN WB. 2012. Real-time observation and prediction of physical processes in a typhoon-affected lake. Paddy and Water Environ 10: 17-30.

KUIK GAM ET AL. 2016. Long-term research challenges in wind energy – a research agenda by the European Academy of Wind Energy, Wind Energ Sci 1: 1-39. https://doi.org/10.5194/wes-1-1-2016.

LEE H, CHUNG S, RYU I & CHOI J. 2013. Three-dimensional modeling of thermal stratification of a deep and dendritic reservoir using ELCOM model. J Hydrol Environ Res 7: 124-133.

LEONARD BP. 1991. The ULTIMATE conservative difference scheme applied to unsteady one-dimensional advection. Comput Methods Appl Mech Eng 88: 17-74.

LISI PJ & SCHINDLER DE. 2015. Wind-driven upwelling in lakes destabilizes thermal regimes of downstream rivers. Limnol Oceanogr 60: 169-180.

LIU M, ZHANG Y, SHI K, ZHANG Y, ZHOU Y, ZHU M, ZHU G, WU Z & LIU M. 2020. Effects of rainfall on thermal stratification and dissolved oxygen in a deep drinking water reservoir. Hydrol Processes 34: 3387-3399.

LORENZZETTI JA, ARAÚJO CAS & CURTARELLI MP. 2015. Mean diel variability of surface energy fluxes over Manso Reservoir. Inland Waters 5: 155-172.

MACINTYRE S, FLYNN KM, JELLISON R & ROMERO JR. 1999. Boundary mixing and nutrient fluxes in Mono Lake, California. Limnol Oceanogr 44: 512-529.

MACINTYRE S, ROMERO JR & KLING GW. 2002. Spatial-temporal variability in surface layer deepening and lateral advection in an embayment of Lake Victoria, East Africa. Limnol Oceanogr 47: 656-671.

MAO H & TALBOT R. 2004. Role of meteorological processes in two New England ozone episodes during summer 2001. J Geophys Res Atmos 109.

MARENGO JA, SOARES WR, SAULO C & NICOLINI M. 2004. Climatology of the Low-Level Jet East of the Andes as Derived from the NCEP-NCAR Reanalyses: Characteristics and Temporal Variability. J Climate 17: 2261-2280.

MIAO Y, GUO J, LIU S, WEI W, ZHANG G, LIN Y & ZHAI P. 2018. The Climatology of Low-Level Jet in Beijing and Guangzhou, China. J Geophys Res Atmos 123: 2816-2830.

MISSAGHI S & HONDZO M. 2010. Evaluation and Application of a Three-Dimensional Water Quality Model in a Shallow Lake with Complex Morphometry. Ecol Model 221: 1512-1525.

MISSAGHI S, HONDZO M & MELCHING C. 2013. Three-dimensional lake water quality modeling: sensitivity and uncertainty analyses. J Environ Qual 42: 1684-1698.

MONISMITH S. 1986. An experimental study of the upwelling response of stratified reservoirs to surface shear stress. J Fluid Mech 171: 407-439.

MONTINI TL, JONESC & CARVALHO LMV. 2019. The South American Low-Level Jet: A New Climatology, Variability, and Changes. J Geophys Res Atmos 124: 1200-1218.

NASH JE & SUTCLIFFE JV. 1970. River flow forecasting through conceptual models part I-A discussion of principles. J Hydrol 10: 282-290.

NASSIF FB, PIMENTA FM, D'AQUINO CA, ASSIREU AT, GARBOSSA LHP & PASSOS JC. 2020. Coastal wind measurements and power assessment using a LIDAR on a pier. Rev Bras Meteorol 35: 255-268.

OLDEN JD & NAIMAN RJ. 2010. Incorporating thermal regimes into environmental flows assessments: modifying dam operations to restore freshwater ecosystem integrity. Freshw Biol 55: 86-107.

PACHECO F, ASSIREU A & ROLAND F. 2011. Derivadores rastreados por satélites aplicados a ambientes aquáticos continentais: Caso do Reservatório de Manso. In Novas tecnologias para o monitoramento e estudo de reservatórios hidrelétricos e grandes lagos (in Portuguese), p. 193-218.

PELLEGRINI CC, ARAUJO C, REIS AL, PIMENTA FM & ASSIREU AT. 2019. Análise do desempenho do modelo WRF num episódio de vento intenso e persistente num grande reservatório tropical. Rev Bras Meteorol 34: 121-138.

PORTÉ-AGEL F, BASTANKHAH M & SHAMSODDIN S. 2020. Wind-Turbine and Wind-Farm Flows: A Review. Boundary-Layer Meteoro 174: 1-59.

REYNOLDS CS. 1992. Dynamics, selection and composition of phytoplankton in relation to vertical structure in lakes. Ergeb Limnol 35: 13-31.

RIFE DL, PINTO JO, MONAGHAN AJ, DAVIS CA & HANNAN JR. 2010. Global Distribution and Characteristics of Diurnally Varying Low-Level Jets. J Climate 23: 5041-5064.

SALIO P, NICOLINI M & ZIPSER EJ. 2007. Mesoscale Convective Systems over Southeastern South America and Their Relationship with the South American Low-Level Jet. Mon Weather Rev 135: 1290-1309.

SCHMID M, BUSBRIDGE M & WÜ EST A. 2010. Double-diffusive convection in Lake Kivu. Limnol Oceanogr 55: 225-238.

SCHMID M, HALBWACHS M, WEHRLI B & WÜEST A. 2005. Weak mixing in Lake Kivu: New insights indicate increasing risk of uncontrolled gas eruption. Geochemistry, Geophysics, Geosystems 6.

SHERMAN FS, IMBERGER J & CORCOS GM. 1978. Turbulence and Mixing in Stably Stratified Waters. Annu Rev Fluid Mech 10: 267-288.

SHINTANI T, DE LA FUENTE A, NIÑO Y & IMBERGER J. 2010. Generalizations of the Wedderburn number: Parameterizing upwelling in stratified lakes. Limnol Oceanogr 55: 1377-1389.

SLATER PN. 1980. Remote sensing: optics and optical systems. In *Reading*. https://ui.adsabs.harvard.edu/abs/1980aw...book.....S.

SPIGEL RH & IMBERGER J. 1987. Mixing processes relevant to phytoplankton dynamics in lakes. N Z J Mar Freshwater Res 21: 361-377.

STECH JL, LIMA IBT, MORAES NOVO E, SILVA CM, ASSIREU AT, LORENZZETTI JA, CARVALHO JC, BARBOSA CC & ROSA RR. 2006. Telemetric monitoring system for meteorological and limnological data acquisition. Internationale Vereinigung Für Theoretische Und Angewandte Limnologie: Verhandlungen 29: 1747-1750.

STEEL EA, TILLOTSON A, LARSEN DA, FULLERTON AH, DENTON KP & BECKMAN BR. 2012. Beyond the mean: The role of variability in predicting ecological effects of stream temperature on salmon. Ecosphere 3: art104.

STENSRUD DJ. 1996. Importance of Low-Level Jets to Climate: A Review. J Climate 9: 1698-1711.

STEVENS CL & LAWRENCE GA. 1997. Estimation of wind-forced internal seiche amplitudes in lakes and reservoirs, with data from British Columbia, Canada. Aquatic Sciences 59: 115-134.

STONE JR, SAROS JE & SPANBAUER TL. 2019. The Influence of Fetch on the Holocene Thermal Structure of Hidden Lake, Glacier National Park. Front Earth Sci 7: 28.

THIERY WIM, STEPANENKO VM, FANG X, JÖHNK KD, LI Z, MARTYNOV A, PERROUD M, SUBIN ZM, DARCHAMBEAU F, MIRONOV D & LIPZIG NPMV. 2014. LakeMIP Kivu: evaluating the representation of a large, deep tropical lake by a set of one-dimensional lake models. Tellus A: Dyn Meteorol Oceanogr 66: 21390.

THOMPSON RORY & IMBERGER J. 1980. Response of a numerical model of a stratified lake to wind stress. In Second International Symposium on Stratified Flows, p. 562-570.

TODD MC, WASHINGTON R, RAGHAVAN S, LIZCANO G & KNIPPERTZ P. 2008. Regional Model Simulations of the Bodélé Low-Level Jet of Northern Chad during the Bodélé Dust Experiment (BoDEx 2005). J Climate 21: 995-1012.

TSAI JW, KRATZ T, HANSON P, WU JT, CHANG W, ARZBERGER P, LIN BS, LIN FP, CHOU HM & CHIU CY. 2008. Seasonal dynamics, typhoons and the regulation of lake metabolism in a subtropical humic lake. Freshw Biol 53: 1929-1941.

TUNDISI JG, MATSUMURA-TUNDISI T, ARANTES JUNIOR JD, TUNDISI JEM, MANZINI NF & DUCROT R. 2004. The response of Carlos Botelho (Lobo, Broa) reservoir to the passage of cold fronts as reflected by physical, chemical, and biological variables. Braz J Biol 64: 177-186.

TUNDISI JG, MATSUMURA-TUNDISI T, PEREIRA KC, LUZIA AP, PASSERINI MD, CHIBA WAC, MORAIS MA & SEBASTIEN NY. 2010. Cold fronts and reservoir limnology: an integrated approach towards the ecological dynamics of freshwater ecosystems. Braz J Biol 70: 815-824.

VASSEUR DA, DELONG JP, GILBERT B, GREIG HS, HARLEY CDG, MCCANN KS, SAVAGE V, TUNNEY TD & O'CONNOR MI. 2014. Increased temperature variation poses a greater risk to species than climate warming. Proc R Soc B: Biol Sci 281: 20132612.

VERA C, HIGGINS W, AMADOR J, AMBRIZZI T, GARREAUD R, GOCHIS D, GUTZLER D, LETTENMAIER D, MARENGO J, MECHOSO CR, NOGUES-PAEGLE J, DIAS PLS & ZHANG C. 2006. Toward a Unified View of the American Monsoon Systems. J Climate 19: 4977-5000.

VERBURG P & ANTENUCCI JP. 2010. Persistent unstable atmospheric boundary layer enhances sensible and latent heat loss in a tropical great lake: Lake Tanganyika. J Geophys Res Atmos 115.

VERBURG P, ANTENUCCI JP & HECKY RE. 2011. Differential cooling drives large-scale convective circulation in Lake Tanganyika. Limnol Oceanogr 56: 910-926.

WAINWRIGHT CE, STEPANIAN PM & HORTON KG. 2016. The role of the US Great Plains low-level jet in nocturnal migrant behavior. Int J Biometeorol 60: 1531-1542.

WALTERS CK, WINKLER JA, SHADBOLT RP, VAN RAVENSWAY J & BIERLY GD. 2008. A Long-Term Climatology of Southerly and Northerly Low-Level Jets for the Central United States. Ann Assoc Am Geogr 98: 521-552.

WEI W, WU BG, YE XX, WANG HX & ZHANG HS. 2013. Characteristics and Mechanisms of Low-Level Jets in the Yangtze River Delta of China. Boundary-Layer Meteorol 149: 403-424.

WOOLWAY RI. 2015. Lake Heat Flux Analyzer user manual.

WOOLWAY RI, JONES ID, HAMILTON DP, MABERLY SC, MURAOKA K, READ JS, SMYTH RL & WINSLOW LA. 2015. Automated

calculation of surface energy fluxes with high-frequency lake buoy data. Environ Model Softw 70: 191-198.

WÜEST A & LORKE A. 2003. SMALL-SCALE HYDRODYNAMICS IN LAKES. Annu Rev Fluid 35: 373-412.

XU L, LIU H, DU Q & WANG L. 2016. Evaluation of the WRF-lake model over a highland freshwater lake in southwest China. J Geophys Res Atmos 121: 914-989.

XU X, YI C & KUTTER E. 2015. Stably stratified canopy flow in complex terrain. Atmos Chem Phys 15: 7457-7470.

ZAMANI B & KOCH M. 2020. Comparison Between Two Hydrodynamic Models in Simulating Physical Processes of a Reservoir with Complex Morphology: Maroon Reservoir. Water 12.

ZEPHIR. 2014. Zephir 300 operations & maitenance manual v3.7. In: Zephir Ltd, p. 64.

ZHAO Y. 2012. Numerical investigation of a localized extremely heavy rainfall event in complex topographic area during midsummer. Atmos Res 113: 22-39.

ZHONG S, FAST JD & BIAN X. 1996. A Case Study of the Great Plains Low-Level Jet Using Wind Profiler Network Data and a High-Resolution Mesoscale Model. Mon Weather Rev 124: 785-806.

How to cite

REIS AL, PACHECO FS, PIMENTA FM, PASSOS RB, FISCH G, MENDONÇA JC & ASSIREU AT. 2023. Effects of atmospheric low-level jets on the mixing process of a large tropical reservoir. An Acad Bras Cienc 95: e20211594. DOI 10.1590/0001-3765202320211594.

Manuscript received on December 18, 2021; accepted for publication January 27, 2023

ANDRÉ L. REIS[1]
https://orcid.org/0000-0002-0744-5489

FELIPE S. PACHECO[2]
https://orcid.org/0000-0003-2143-5225

FELIPE M. PIMENTA[3]
https://orcid.org/0000-0002-0748-9182

ROBSON B. PASSOS[1]
https://orcid.org/0000-0002-3798-5953

GILBERTO FISCH[4]
https://orcid.org/0000-0001-6668-9988

JOSÉ C. MENDONÇA[5]
https://orcid.org/0000-0001-9894-9369

ARCILAN T. ASSIREU[1]
https://orcid.org/0000-0002-4237-2449

[1]Universidade Federal de Itajubá/UNIFEI, Instituto de Recursos Naturais, Av. BPS, 1303, Pinheirinho, 37500-903 Itajubá MG, Brazil

[2]Department of Ecology and Evolutionary Biology, Cornell University, Tower Rd, 2015, Ithaca, 14853 New York, USA

[3]Programa de Pós-Graduação em Oceanografia, Universidade Federal de Santa Catarina/UFSC, Rua Eng. Agronômico Andrei Cristian Ferreira, s/n, Trindade, 88040-900 Florianópolis, SC, Brazil

[4]Universidade de Taubate/UNITAU, Departamento de Ciências Agrárias, Rua Quatro de Março, 432, Centro, 12020-270 Taubaté, SP, Brazil

[5]Universidade Estadual do Norte Fluminense Darcy Ribeiro, Labortório de Engenharia Agrícola/LEAG, Av. Brennand, s/n, Imboassica, 27925-535 Macaé, RJ, Brazil

Correspondence to: **André L. Reis**
E-mail: andreluiz.reis4@gmail.com

Author contributions

André L. Reis - conceptualization, data collection, data curation, formal analysis, investigation, methodology, software, writing-original draft, writing-review & editing. **Felipe S. Pacheco** - conceptualization, data collection, formal analysis, investigation, methodology, software, supervision, writing-original draft, writing-review & editing. **Felipe M. Pimenta** - conceptualization, data collection, investigation, methodology, writing-review & editing. **Robson B. Passos and Gilberto Fisch** - conceptualization, methodology, writing-review & editing. **José Carlos Mendonça -** data collection, methodology. **Arcilan T. Assireu** - conceptualization, data collection, formal analysis, methodology, project administration, supervision, writing-original draft, writing-review & editing.